Translational Oncology 25 (2022) 101519

Contents lists available at ScienceDirect

Translational Oncology

journal homepage: www.elsevier.com/locate/tranon

Original Research

Construction and validation of a novel ten miRNA-pair based signature for the prognosis of clear cell renal cell carcinoma

Yulin Wang [a,b,c,1], Ziyan Shen [a,b,d,1], Shaocong Mo [e,1], Leijie Dai [f], Biao Song [g], Wenchao Gu [h], Xiaoqiang Ding [a,b,c,d,**], Xiaoyan Zhang [a,b,c,d,*]

[a] Department of Nephrology, Zhongshan Hospital, Fudan University, No. 180 Fenglin Road, Shanghai 200032, China
[b] Shanghai Medical Center of Kidney Disease, Shanghai 200032, China
[c] Shanghai Key Laboratory of Kidney and Blood Purification, Shanghai 200032, China
[d] Shanghai Institute of Kidney and Dialysis, No. 136 Medical College Road, Shanghai 200032, China
[e] Department of Digestive Diseases, Huashan Hospital, Fudan University, Shanghai 200040, China
[f] Department of Breast Surgery, Fudan University Shanghai Cancer Center, Shanghai 200032, China
[g] Department of Dermatology, Peking Union Medical College Hospital, Beijing, 100005, China
[h] Department of Diagnostic Radiology and Nuclear Medicine, Gunma University Graduate School of Medicine, Maebashi, 371-8511, Japan

ARTICLE INFO

Keywords:
miRNA-pair
ccRCC
Prognosis
Signature
Immune
Bioinformatics

ABSTRACT

Background: Clear cell renal cell carcinoma (ccRCC) is the most predominate pathological subtype of renal cell carcinoma, causing a recurrence or metastasis rate as high as 20% to 40% after operation, for which effective prognostic signature is urgently needed.
Methods: The mRNA and miRNA profiles of ccRCC specimens were collected from the Cancer Genome Atlas. MiRNA-pair risk score (miPRS) for each miRNA pair was generated as a signature and validated by univariate and multivariate Cox proportional hazards regression analysis. Functional enrichment was performed, and immune cells infiltration, as well as tumor mutation burden (TMB), and immunophenoscore (IPS) were evaluated between high and low miPRS groups. Target gene-prediction and differentially expressed gene-analysis were performed based on databases of miRDB, miRTarBase, and TargetScan. Multivariate Cox proportional hazards regression analysis was adopted to establish the prognostic model and Kaplan-Meier survival analysis was performed.
Findings: A novel 10 miRNA-pair based signature was established. Area under the time-dependent receiver operating curve proved the performance of the signature in the training, validation, and testing cohorts. Higher TMB, as well as the higher CTLA4-negative PD1-negative IPS, were discovered in high miPRS patients. A prognostic model was built based on miPRS (1 year-, 5 year-, 10 year- ROC-AUC=0.92, 0.84, 0.82, respectively).
Interpretation: The model based on miPRS is a novel and valid tool for predicting the prognosis of ccRCC.
Funding: This study was supported by research grants from the China National Natural Scientific Foundation (81903972, 82002018, and 82170752) and Shanghai Sailing Program (19YF1406700 and 20YF1406000).

Introduction

Renal cell carcinoma (RCC) is one of the most lethal malignant tumor in urinary system, with a rising incidence and poor prognosis [1,2]. It was reported that the 5-year survival of RCC was 76% in the US [3]. However, the survival rate is highly dependent on the diagnosis stage, with a 5-year relative survival rate of 93% in stage I, 72.5% in stage II/III regional diseases, and only 12% in stage IV metastatic diseases [4].

Clear cell renal cell carcinoma (ccRCC) is the most predominate pathological subtype of RCC in approximately 80% of all cases [5,6]. Since there are no perceptible symptoms and signs in the early stage of ccRCC, more than one third of patients were found with distant metastasis at the time of diagnosis [7]. As ccRCC is resistant to traditional radiotherapy and chemotherapy, and mRCC targeted therapy is

* Corresponding author at: Shanghai Institute of Kidney and Dialysis, No. 136 Medical College Road, Shanghai 200032, China.
** Corresponding author at: Department of Nephrology, Zhongshan Hospital, Fudan University, No. 180 Fenglin Road, Shanghai 200032, China.
E-mail addresses: ding.xiaoqiang@zs-hospital.sh.cn (X. Ding), zhang.xiaoyan@zs-hospital.sh.cn (X. Zhang).
[1] These authors contributed equally to this work.

https://doi.org/10.1016/j.tranon.2022.101519
Received 11 April 2022; Received in revised form 12 July 2022; Accepted 10 August 2022

expensive, radical or partial nephrectomy have become the most common treatment for ccRCC [8–11]. Although ccRCC can be effectively resolved by surgical resection, the local recurrence or distant metastasis is still as high as 20% to 40% after operation [12]. Meanwhile, it is difficult to predict the outcome of patients accurately, despite a number of grading systems contributing to forming prognostic models, such as TNM staging system, Necrosis (SSIGN) Risk Score, Fuhrman grading and the University of California Los Angeles Integrated Staging System (UISS) [13–17]. Thus, it is crucial to screen out sensitive biomarkers and construct accurate prognosis models for early diagnosis and improvement of prognosis.

Recent studies suggest that a number of miRNAs are relevant to the development of ccRCC, including proliferation, invasion, migration, apoptosis, and carcinogenesis [18–20]. The aberrant expression of some miRNAs between ccRCC and the normal samples has been universally measured, presenting its value as marker in diagnosis, predicting

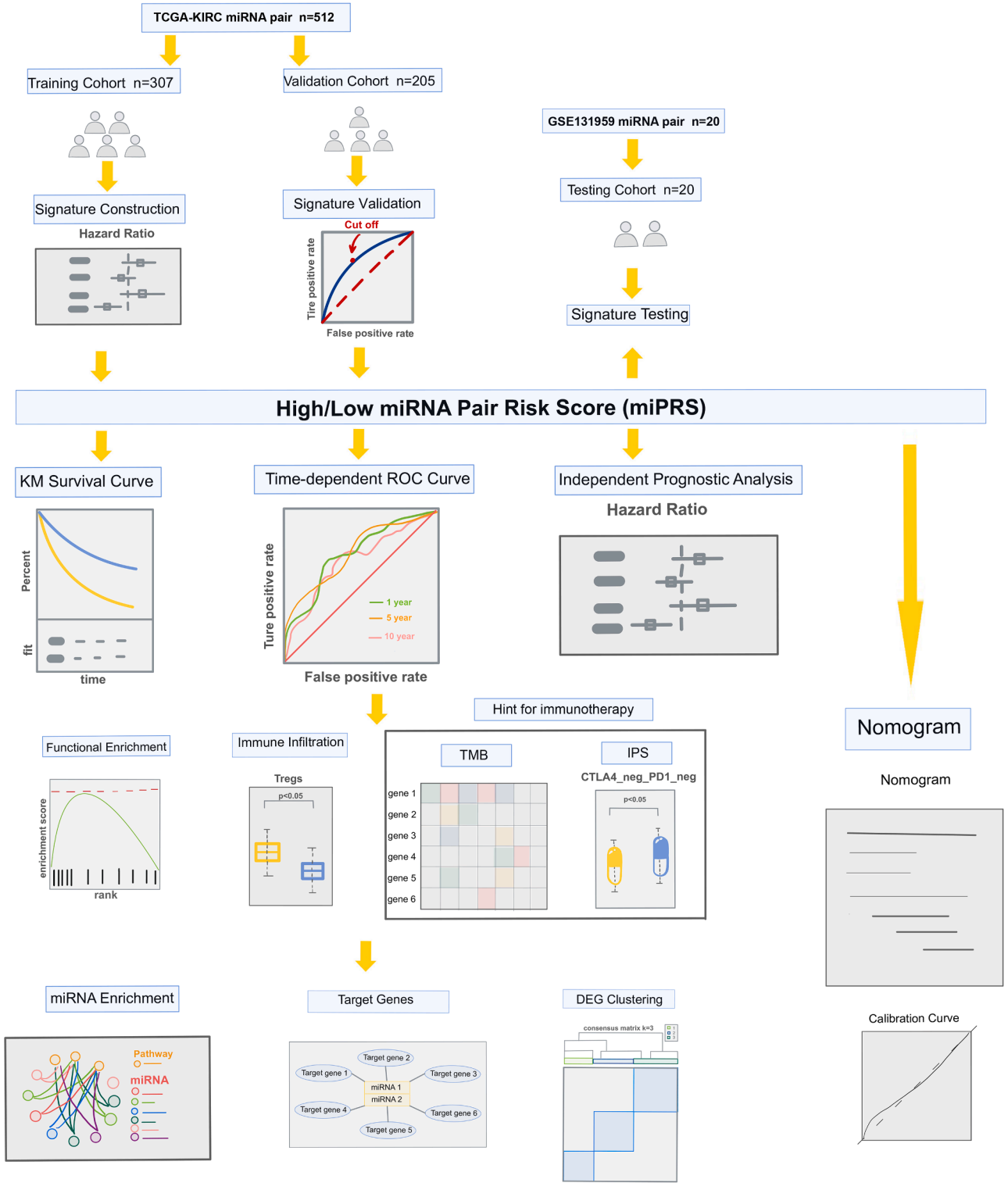

Fig. 1. Work flow chart of the study.

prognosis, or potential therapeutic targets [21–23]. Nowadays, more and more studies applying gene and miRNA pairs risk signatures are used to predict the prognosis of different kinds of tumors [24–27]. However, due to the differences in testing or quantitative methods (miRNA-seq, microarray or qRT-PCR) and histological variations in study cohort, the effectiveness of miRNAs serving as prognosis biomarkers is controversial in clinical practice.

Although there are many ccRCC prognostic models based on transcriptome study, there is still an urgent need to explore the disease from an overall perspective. MiRNA is an upstream regulatory factor contained in limited numbers within the cell. Expression levels can reflect the overall state of the cell. We introduced the concept of miRNA pairs with the aim of constructing an unprecedented prognostic model of ccRCC that is widely generalized, robust, and stable. Inspired by the above observations, we tried to find a robust and novel model based on miRNA to predict the prognosis of ccRCC, which may provide new aspects for clinical treatment and pathological mechanism exploration of the disease. In the present study, we adopted the method of miRNA pair, and established a signature of ten miRNA pairs [28]. The miRNA-pair risk score (miPRS) was calculated and data of multiple -omics between high and low miPRS groups were compared, including gene expression, immune cell infiltration, tumor mutation burden, immunophenoscore, and drug sensitivity score. Our research has pioneering significance in the treatment and prognosis of ccRCC.

Methods

Work flow

The work flow of the study was as Fig. 1 showed.

Data collection and cohort partition

The mRNA and miRNA profiles of 537 specimens of ccRCC were obtained from the database of "The Cancer Genome Atlas-Kidney Renal Clear Cell Carcinoma" (TCGA-KIRC, https://portal.gdc.cancer.gov/). A total of 512 specimens equipped with survival information and other clinical data were included in our study. The ratio of 6:4 was employed to divide the 512 samples into training cohort and validation cohort at random. Demographic baseline data is shown in Table 1. We also gained the variant aggregation and masking data of KIRC patients (n=336) from TCGA database (TCGA-KIRC, https://portal.gdc.cancer.gov/).

The miRNA profile of 20 samples of ccRCC from GSE131959 were downloaded from Gene Expression Omnibus (GEO, https://www.ncbi.nlm.nih.gov/geo/), as well as the survival data and other clinical baseline features [29].

Intersection of miRNA from TCGA-KIRC and GSE131959 was performed to construct the miRNA pairs and signature, which refers to the miRNAs equipped with -3p or -5p modification based on miRbase manually [30].

Signature construction and validation

The expression levels of candidate miRNAs were compared in pairs to generate a score for each miRNA pair. If the expression level of the first miRNA in a certain sample was less than the second miRNA, the value of the pair in the sample was set to 0, otherwise the value was set to 1. Only miRNA pairs with a value of 1 in 20% to 80% of samples were included in the study [25,26]. Univariate Cox proportional hazards regression analysis was performed to explore the correlation between the miRNA pairs and the overall survival outcomes. In the training cohort, with the p-value set to 0.01, Least Absolute Shrinkage and Selection Operator (LASSO) Cox regression analysis was performed to reduce the scale of miRNA pairs included in the signature. The best log (λ) was produced by 10 folds cross-validation.

Based on the selected miRNA pairs, multivariate Cox proportional hazards regression analysis was performed with a backward stepwise regression. The selected miRNA pairs were considered as covariates and the overall survival states were regarded as the only outcome. Subsequently, the miRNA-pair risk score(miPRS) of each sample was calculated based on this signature. The cutoff of miPRS was determined by the highest point of the ROC curve of the TCGA training cohort, where the signature has the highest prognostic power according to the definition of the ROC curve. In addition, the same cutoff value to validate the model was used in the TCGA testing cohort and GEO validation cohort. Kaplan - Meier survival curve and time-dependent ROC curve were generated and both univariate and multivariate Cox proportional hazards regression analysis were performed. Overall survival state was regarded as the only outcome in all Cox proportional hazards regression analysis.

Table 1
Demographic and baseline clinical features of the training, validation and testing cohorts.*

Variables		Training Cohort N=307	Validation Cohort N=205	GEO Testing Cohort (GSE131959) N=20
		n(%)	n(%)	n(%)
Age				
	<65	204 (66.45)	119 (58.05)	12(60.00)
	>=65	103 (33.55)	86(41.95)	8(40.00)
Gender				
	male	200 (65.15)	113 (55.12)	/
	female	107 (34.85)	72(35.12)	/
Grade				
	G1	7(2.28)	6(2.93)	2(10.00)
	G2	136 (44.30)	79(38.54)	3(15.00)
	G3	110 (35.83)	91(44.39)	11(55.00)
	G4	48(15.64)	27(13.17)	4(20.00)
	GX	4(1.30)	1(0.49)	0
	unknown	2(0.65)	1(0.49)	0
Stage				
	Stage I	161 (52.44)	90(43.90)	20 (100.00)
	Stage II	32(10.42)	22(10.73)	0
	Stage III	67(21.82)	55(26.83)	0
	Stage IV	45(14.66)	37(18.05)	0
	unknown	2(0.65)	1(0.49)	0
Survival Status				
	Alive	218 (71.01)	129 (62.93)	14(70.00)
	Dead	89(28.99)	76(37.07)	6(30.00)

* 65 was chosen as the cutoff value of age based on previous literature [88–93].

Functional enrichment

Gene Ontology (GO) database is a widely used ontology in the field of bioinformatics, which covers thousands of terms from three aspects of biology: Cellular Component (CC), Molecular Function (MF), and Biological Process (BP) [31]. Kyoto Encyclopedia of Genes and Genomes (KEGG) is a database used to understand the advanced functions and utility of biological systems [32]. Gene Set Enrichment Analysis (GSEA) is an analysis method for genome-wide expression profile chip data, which compares genes with predefined gene sets and analyzes gene expression profile data in order to understand their expression status in specific functional gene sets and their statistically significance [33]. "fgsea" package was used to perform the GSEA. The R package of "clusterProfiler" was applied to conduct GO and KEGG enrichment

analysis with p-value filter set to 0.05 and q-value filter set to 1, after which "enrichplot" and "ggplot2" packages were employed to visualize the results of enrichment analysis by showing the enriched functions and pathways [34]. Additionally, miEAA (http://ccb-compute2.cs.uni-saarland.de/mieaa2/) was used for miRNA functional enrichment [35].

Immune cells infiltration evaluation

CIBERSORT (A R script version) was applied to obtain the infiltration levels of 22 kinds of immune cells in the sample, including memory B cells, naive B cells, activated dendritic cells, resting dendritic cells, eosinophils, macrophages M0, macrophages M1, macrophages M2, activated mast cells, resting mast cells, resting NK cells, plasma cells, activated memory CD4 T cells, naive CD4 T cells, resting memory CD4 T cells, monocytes, neutrophils, activated NK cells, CD8 T cells, T follicular helper cells, regulatory T cells (Tregs), and activated memory CD4 T cells, etc. [36]. We applied Wilcoxon signed-rank test to each type of immune cell to judge whether there was a significant difference in the infiltration level between high and low miPRS groups. The "fmsb" package was used to visualize the results in a radar chart.

Tumor mutation burden (TMB) and immunophenoscore (IPS)

The intersection of the patients with variant aggregation and masking data (n=336) and patients included in the training and validation cohorts (n=512) with survival data were used to conduct the TMB analysis (n=196). We used the "maftools" package to process the variant aggregation and masking data from TCGA, and the top 30 most significant mutated genes with different mutation categories were visualized by an onco-plot [37]. Next, the TMB of each sample was calculated, and four new groups (H-TMB&H-RISK, H-TMB&L-RISK, L-TMB&H-RISK, L-TMB&L-RISK) were generated after integration with the miPRS.

IPS of TCGA-KIRC patients (n=533), z-scores from 0 to 10, were obtained from TCIA (the cancer-immune group atlas) (https://tcia.at/home), which contained the information of the two categories of immunogenicity-determining genes: CTLA-4 and PD-1. The IPS in high and low risk groups were then compared. The intersection of the patients with IPS data (n=533) and patients included in training and validation cohort (n=512) with survival data were used to conduct the IPS analysis (n=152).

Target gene-prediction and differentially expressed gene-analysis

We used the intersection of three distinguished databases: miRDB, miRTarBase, and TargetScan, to predict the downstream target genes of selected miRNA. Only genes identified in all three databases were considered as target genes [38–40]. Cytoscape was used to visualize the miRNA-mRNA network [41].

Differentially expressed genes between high (upper quantile) and low (lower quantile) miPRS were screened out with "limma" package ($|\log2Foldchange| \geq 1$, adjusted P value<0.01) [42]. We then took the intersection of the downstream target genes and the DEGs to generate target-DEGs, and evaluate the target-DEGs' prognostic value and correlations with immune cells.

Furthermore, we used the "ConsensusClusterPlus" package to classify genes using the k-means algorithm and euclidean to calculate the distance [43]. After clustering with the best number of clusters, we again compare the differences of OS and immune infiltration between the subgroups, as described above.

Drug sensitivity evaluation

Drug sensitivity data and gene expression profile of three widely-known databases, CellMiner (NCI-60), GDSC, and CCLE, were downloaded from their official websites [44–46].

CellMiner (NCI-60) is a database (https://discover.nci.nih.gov/cellminer/home.do) that contains comparison of transcript expression levels of 22,217 genes, 360 microRNAs, and 18,549 compounds including 91 Food and Drug Administration (FDA)-approved drugs [47]. This database can be employed to explore transcript and drug patterns in the NCI-60 cell line set. The US National Cancer Institute 60 human tumor cell line (NCI-60) anticancer drug screen has been used for *in vitro* drug study of anticancer drug activity, genomic, molecular, and phenotypic data in order to replace the use of transplantable animal tumors in anticancer drug screening [48]. We downloaded transcriptome sequencing data and drug susceptibility testing data of the NCI-60 cell line from the database, where the susceptibility of various cells to drugs is indicated by $\log_{10}$ (half maximal growth inhibition), abbreviated as $\log_{10}$ (GI50).

The Genomics of Drug Sensitivity in Cancer (GDSC) database (www.cancerRxgene.org) is the largest public resource for information on drug sensitivity in cancer cells and molecular markers of drug response, in which data can be available for free [45]. GDSC database contains drug sensitivity information for 75000 experiments and response to 138 anticancer drugs across 700 cancer cell lines [49]. The transcriptome sequencing data and drug susceptibility testing data were downloaded from the database, and the susceptibility of various cells to drugs is measured by half maximal inhibitory concentration, referred to as IC50.

Cancer Cell Line Encyclopedia (CCLE) database (https://sites.broadinstitute.org/ccle) is made up with a compilation of gene expression, chromosomal copy number, and massively parallel sequencing data from 947 human cancer cell lines [50]. The database provides identification of genetic, lineage, and gene expression-based predictors of drug sensitivity in addition to pharmacologic profiles for 24 anticancer drugs across 479 of the cell lines [51]. The transcriptome sequencing data and drug susceptibility testing data are available from the database, and the susceptibility of various cells to drugs is represented by IC50.

For CellMiner, we evaluate the correlation between target-DEGs and common chemotherapy drugs for ccRCC both in renal carcinoma cell lines and pan-cancer cell lines. For GDSC, we calculate the correlation between target-DEGs and common chemotherapy drugs for ccRCC in pan-cancer cell lines. For CCLE, ccRCC cell lines were selected to evaluate the correlation between target-DEGs and all of the 22 drugs in the database.

Statistical analysis

Signature construction and validation were mediated by the "survival", "glmnet", "surviminer" etc., as described in previous studies [52]. Kaplan-Meier analysis and Log rank test were applied in survival analysis. Wilcoxon signed-rank test was used to compare the median value and Spearman correlation analysis was used to identify the relationship. The upper and lower quartiles of the risk score were applied when necessary. ROC-AUC, nomogram and calibrate curve were used for effectiveness assessment [53,54]. Analysis was done by R version 4.0.5 (http://www.R-project.org/). Website tool hiplot (https://hiplot.com.cn/) and GEPIA (http://gepia.cancer-pku.cn/) were utilized when necessary [55].

Role of funders

Shen Ziyan reviewed and revised the manuscript. Zhang Han served as scientific advisors and supervised data analysis. Zhang Xiaoyan and Ding Xiaoqiang were co-investigators and supervisors of the study.

Results

Signature construction and validation

After intersection, a total of 168 miRNAs were adopted and 14028 miRNA pairs were built, among which 508 were selected to construct the signature. Univariate Cox proportional hazards regression analysis was

conducted in the training cohort and 68 miRNA pairs related to the survival outcomes were screened out. By LASSO Cox regression analysis, the scale of miRNA pairs was reduced to 30 (Fig. 2a-b). Multivariate Cox proportional hazards regression analysis finally determined 10 miRNA pairs and their hazard ratios to constitute the signature (Fig. 2c), including hsa-miR-200b-3p | hsa-miR-342-3p, hsa-miR-215-5p | hsa-miR-223-3p, hsa-miR-139-5p | hsa-miR-193a-3p, hsa-miR-34c-5p | hsa-miR-431-5p, hsa-miR-148b-3p | hsa-miR-144-3p, hsa-miR-411-5p | hsa-miR-504-5p, hsa-miR-190a-5p | hsa-miR-454-3p, hsa-miR-330-5p | hsa-miR-130b-3p, hsa-miR-150-5p | hsa-miR-155-5p and hsa-miR-125a-3p | hsa-miR-183-5p.

Based on signature, each of the 307 specimens in the training cohort was equipped with a miRNA-pair risk score (miPRS), after which the Kaplan-Meier survival analysis was used to demonstrate the difference of the survival outcomes between high and low miPRS groups with 1.4 as a temporary cutoff value (Fig. 2d). Time-dependent ROC curve showed the Area Under Curve (AUC) of the 1-, 5-, and 10-year were 0.81, 0.80 and 0.79 respectively (Fig. 2e). The contrast of demographic and baseline clinical features between high and low miPRS groups showed that, besides miPRS, gender, grade, and stage also have significant difference between the two groups (Table 2).

In the validation process, the signature acquired by training cohort was applied to the validation cohort (n=205) to get the miPRS of each patient. With the cutoff value of 1.4, Kaplan-Meier survival analysis showed the different survival outcomes between high miPRS group (n=80) and low miPRS groups (n=125) (Fig. 2f), and 1.4 was considered as the best cutoff value to divide the cohort into high and low miPRS groups, which was regarded as the final best cutoff threshold. The Area

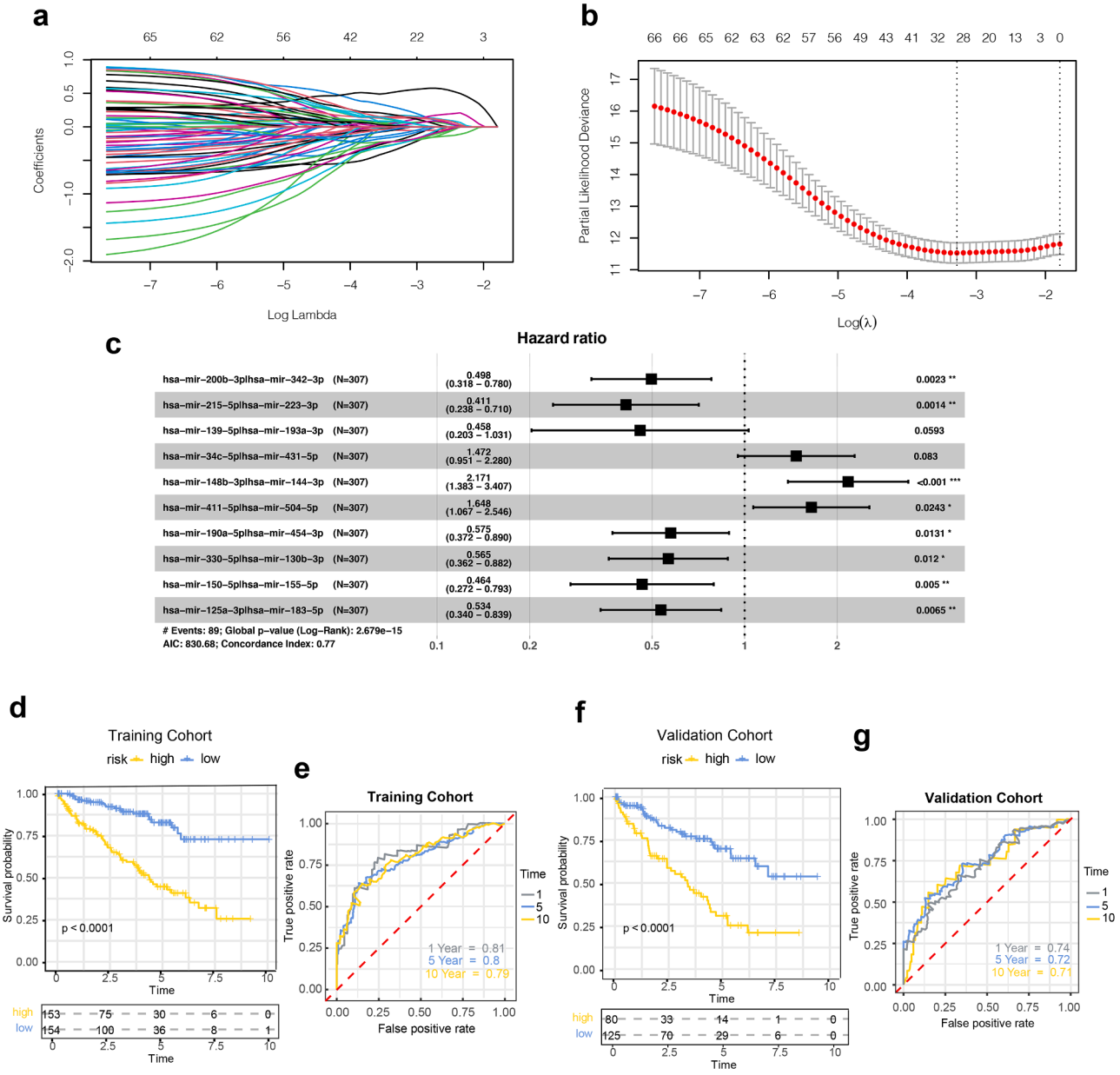

Fig. 2. Signature construction and validation. (a-b) The Least Absolute Shrinkage and Selection Operator (LASSO) Cox regression analysis were carried out. (a) The coefficients of 68 miRNA pairs selected from univariate Cox proportional hazards regression analysis in the training cohort (n=307) vary in the penalized value. (b) The best log (λ) was determined by 10 folds cross-validation. (c) Multivariate Cox proportional hazards regression analysis filtered the pairs to 10 to construct the signature. (d) Kaplan-Meier survival analysis of training cohort (n=307) stratified by 1.4. (e) Time-dependent ROC curve of the training cohort (n=307). (f) Kaplan-Meier survival analysis of validation cohort (n=205) stratified by the best cut off value 1.4 of validation cohort (n=205). (g) Time-dependent ROC curve of the validation cohort (n=205) to evaluate the signature.

Table 2
Demographic and baseline clinical features between high and low miPRS groups*

	High miPRS N=153 n (%)	Low miPRS N=154 n (%)	p value
Age			
<65	95(62.09)	109(70.78)	0.107
>=65	58(37.91)	45(29.22)	
Gender			
male	109(71.24)	91(59.09)	0.0255
female	44(28.76)	63(40.91)	
Grade			
G1~2	51(33.33)	92(59.74)	<0.0001
G3~4	100(65.36)	58(37.66)	
GX	2(1.31)	2(1.30)	
Stage			
Stage I~II	72(47.06)	121(78.57)	<0.0001
Stage III~IV	80(52.29)	32(20.78)	
unknown	1(0.65)	1(0.65)	
Survival Status			
Alive	84(54.90)	134(87.01)	<0.0001
Dead	69(45.10)	20(12.99)	

* Specimens with grade or stage unknown were not included in the analysis.

Under Curve (AUC) of the time-dependent ROC curve of 1-, 5-, and 10-year was 0.74, 0.72 and 0.71, respectively (Fig. 2g).

Signature testing and evaluation

By univariate and multivariate independent prognosis Cox regression analysis, miPRS was an independent factor influencing the survival outcomes in both training and validation cohort (Fig. 3a-d). Moreover, the signature was also applied to the GEO testing cohort (n=20), and stratified the specimens into high miPRS group (n=5), and low miPRS group (n=15) with cutoff value of 1.4. The Kaplan-Meier survival analysis presented obvious different survival consequences between the two groups (p=0.0045) (Fig. 3e), and both univariate and multivariate independent prognosis Cox regression analysis showed miPRS was an independent factor affecting OS (HR 2.519, 95%CI 1.076−5.894, p-value = 0.033; HR 3.921, 95%CI 1.015−15.142, p-value = 0.047) (Fig. 3f, g).

Implementation of gene set enrichment analysis (GSEA) and immune cells infiltration evaluation

We employed Gene Set Enrichment Analysis (GSEA) with GO gene set as reference gene set to find out the significant biological pathways between high and low miPRS groups. In the training cohort specimens were arranged in order of miPRSs. Samples with miPRSs of the highest 25% (n=75) and the lowest 25% (n=75) were selected to carry out GSEA with p-value filter set to 0.05. A total of 34 pathways were found (Table S1), and pathways with the top 10 Normalized Enrichment Scores (NESs) were demonstrated in the bubble plot, including antigen binding, immunoglobulin complex, immunoglobulin receptor binding, etc. (Fig. 4a, Table S1). Partial GSEA results are shown in Fig. 4c. In addition to the validation cohort, specimens with miPRSs of the highest 25% (n=51) and lowest 25% (n=50) were selected to implement GSEA, and 125 pathways were determined. The pathways with the highest 10 NESs, such as antigen binding, immune response by circulating immunoglobulin, B cell mediated immunity, etc., are visualized in the bubble plot (Fig. 4b, Table S2).

Then, CIBERSORT was employed to assess 22 types of immune cells infiltration. The difference of immune cell infiltration between high and low miPRS group in the training cohort are presented in the radar chart (Fig. 4e). The radar chart illustrated that infiltration of T cells regulatory (Tregs), Macrophages M0, and T cells CD4 memory activated were significantly upregulated in high miPRS group while dendritic cells resting was in contrast, which are intuitively presented through the box plots (Fig. 4d). Similar outcomes were confirmed in the validation cohort, whose radar chart and box plots turned out to be consistent with the training cohort (Fig. 4f, g).

Tumor mutation burden (TMB) and immunophenoscore (IPS)

Tumor Mutation Burden (TMB) analysis was conducted for 50 specimens with the highest miPRSs and 50 specimens with the lowest miPRSs in the training cohort. The high miPRS group tended to have a higher TMB rate (median: 0.86 [95% CI: 0.64- 1.06] vs. 0.74[95% CL:0.50-1.01]) (Fig. 5d) and samples from two groups shared the same most common mutated genes, while the high miPRS group showed more missense mutation and less frame shift mutation rate of gene VHL than the low miPRS group. Furthermore, samples of the low miPRS group were inclined to display a higher mutation rate in gene PBRM1 (8% vs 4% in high miPRS group), mainly in form of frame shift mutation (Fig. 5a, b). By Kaplan-Meier survival analysis, samples with both low miPRSs and low TMB had much better prognosis than those with both high miPRSs and high TMB (Fig. 5c). IPS analysis illustrated that the low miPRS group was prone to have higher IPSs than the high miPRS group in samples of both CTL4 and PD1 negative (Fig. 5e).

miRNA Enrichment analysis and target gene prediction combined with differential expressed gene (DEG) analysis

In order to clarify the detailed down-stream mechanism of the miRNAs in our signature, we conducted enrichment analysis onto the 20 miRNAs involved in the 10-miRNA-pair signature, basing on miEEA database, and ascertained five pathways with significant relation to immune response and regulation, consisting of B cell differentiation, leukocyte migration, Ras protein signal transduction, receptor complex, and T cell receptor signaling pathway (Fig. 6a). To determine the target of the miRNAs, databases including miRDB, miRTarBase and TargetScan were employed to predict the target genes of the 20 miRNAs, and 621 genes were consistent in all the databases. We then employed univariate Cox proportional hazards regression analysis to pick the 118 genes strongly correlating with survival prognosis to construct the ceRNA networks (Fig. 6b).

Furthermore, samples with the highest and lowest 25% miPRSs in the training cohort (n=150) were used to conduct the Differential Expressed Gene (DEG) analysis and 839 DEGs were finally determined, which shared a 21-gene intersection with the target genes (Fig. 6c). Overall Survival (OS) and Disease-Free Survival (DFS) analysis were carried out on the 21 most important genes, consisting of FRMD3, MAPT, PANK1, RRAGD, CYB5A, KLF6, GRB10, EZR, KDR, PODXL, ZNF711, PLAU, GRIK3, RHOB, S1PR1, ENPP5, CD36, FLT1, EDN1, F3 and PRUNE2, and most of the genes were confirmed to have higher expression levels in samples with better prognosis (Fig. 6d, Supplementary Figs. 1, 2).

Heatmap of correlation between 21 genes with 22 types of immune cells infiltration in Supplementary Fig. 3a demonstrated many of the 21 genes had an obvious relationship with T cells regulatory (Tregs). Spearman Correlation Analysis were subsequently conducted between the 21 genes and T cells regulatory (Tregs). Three genes (KLF6, PANK1 and RRAGD) that significantly and strongly correlated with T cells regulatory (Tregs) were screened out with |Spearman correlation coefficient| > 0.4 and p-value <0.001 (Fig. 6e, Supplementary Fig. 3a).

Drug sensitivity analysis

In order to determine the relationship between the 21 genes and antitumor drugs from both ccRCC and pan-cancer cases, database including CCLE, CellMiner, and GDSC were used and the correlation coefficients were calculated through Spearman Correlation Analysis. In ccRCC cases, higher expression levels of gene RRADG, RGB10, and EZR

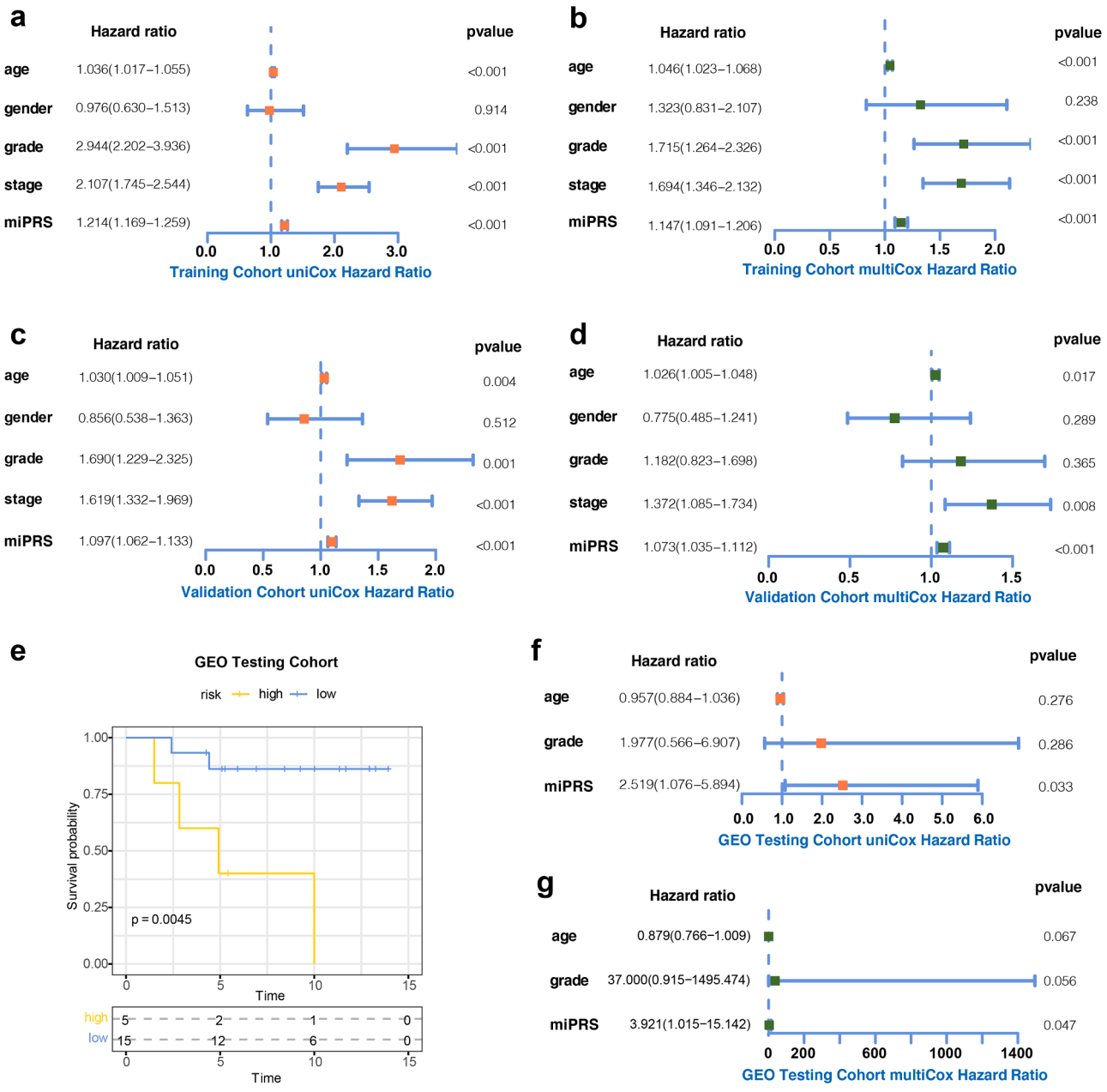

Fig. 3. Signature validation and evaluation. (a) Univariate Cox regression analysis was conducted in the training cohort (n=307) to judge whether miPRS, age, gender, grade and stage are independent prognostic factors (b) Multivariate independent prognosis Cox regression analysis were conducted in the training cohort (n=307) to find out the judge whether miPRS, age, gender, grade and stage are independent prognostic factors. (c) Univariate independent prognosis Cox regression analysis of validation cohort (n=205). (d) Multivariate independent prognosis Cox regression analysis of validation cohort (n=205). (e) Kaplan-Meier survival analysis of GEO testing cohort (n=20) stratified by the signature. (f) Univariate independent prognosis Cox regression analysis of GEO testing cohort (n=20). (g) Multivariate independent prognosis Cox regression analysis of GEO testing cohort (n=20).

tended to have a positive effect on certain antitumor drugs, such as ZD-6474, RAF265, Temsirolimus and Everolimus, and Panobisonstat was prone to be more sensitive to cases with more expression of RRAGD and ENPD5 (Fig. 7a, b). Of particular note is that gene FTL1 tended to have a positive impact on the all 8 types of drugs involved, which indicates an increase of drug sensitivity to pan-cancer specimens with higher expression levels of FTL1 (Fig. 7c, d).

Differential expressed genes (DEGs) enrichment and clustering analysis

To confirm the reliability of our signature, DEGs found in the above section 3.5 were applied to determine the clusters of the patients. First, GO and KEGG enrichment analysis impacted pathways strongly related to immune response and regulation like complement activation classical pathway, immunoglobulin complex and immunoglobulin receptor binding, etc., which were consistent with the above results (Fig. 8a). Univariate Cox proportional hazards regression analysis helped to select 531 prognosis-related DEGs, based on gene clustering analysis and 3 subgroups were determined (Fig. 8b, Supplementary Fig. 3b). Kaplan-Meier survival analysis illustrated a significant difference among the 3 classes; class B had the best prognosis while class C had the worst (Fig. 8c). This could also be confirmed and explained by the boxplot in which specimens of class B had the highest miPRSs and class C had the lowest ones (Fig. 8d). Additionally, immune cells infiltration analysis also presented that class C had a higher infiltration level of T cells regulatory (Tregs) while class B had the least infiltration (Fig. 8e).

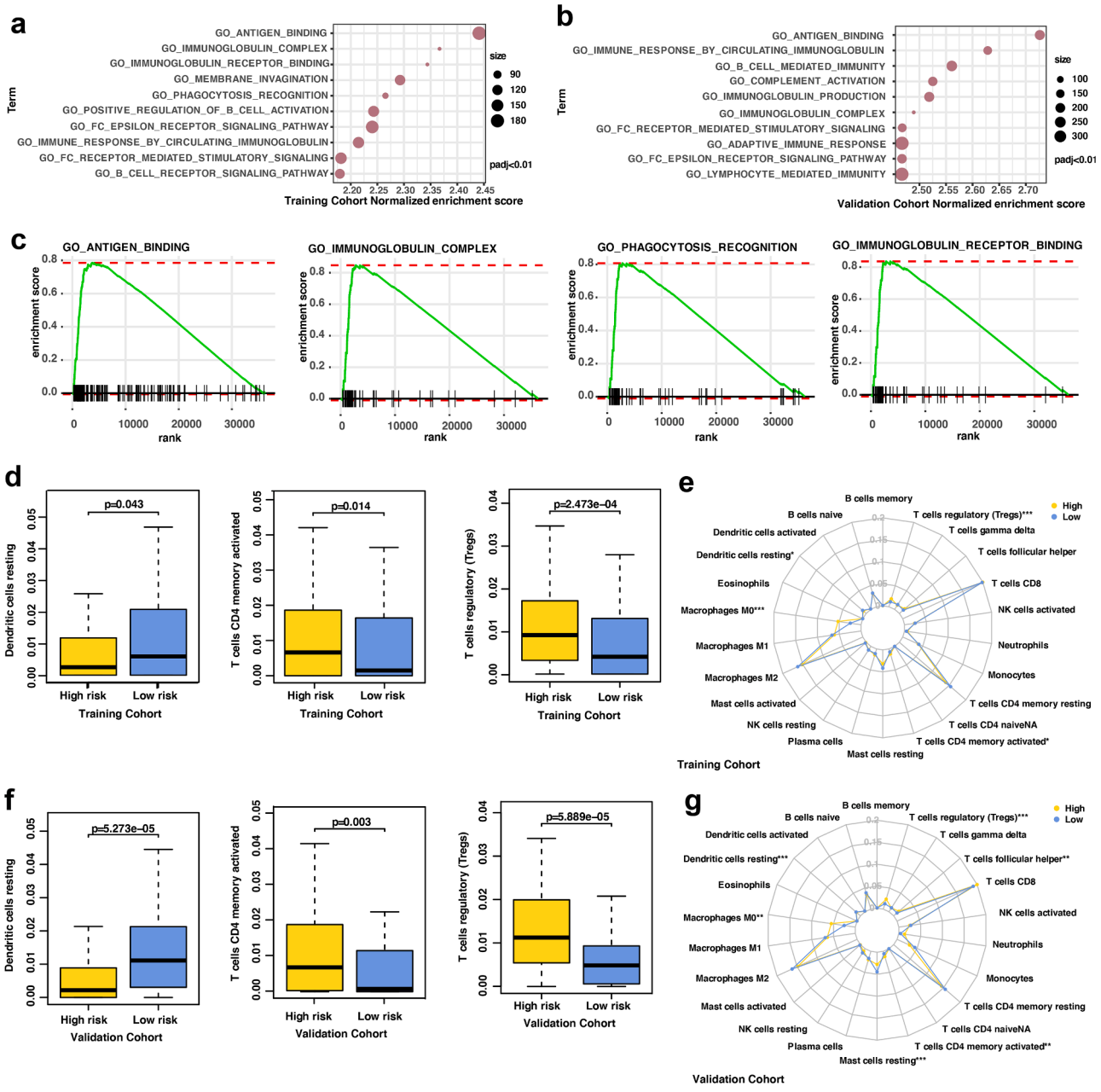

Fig. 4. Functional enrichment analysis and immune cells infiltration evaluation. (a) Bubble chart of GO enrichment results of training cohort (n=150) from gene-set enrichment analysis (GSEA). (b) Bubble chart of GO enrichment results of validation cohort (n=101) from gene-set enrichment analysis (GSEA). (c) Partial outcomes of GSEA shared in training and validation cohort. (d) Partial results of immune cells infiltration evaluation between high and low miPRS in the training cohort (n=208). (e) Radar chart to evaluate infiltration of 22 types of immune cells between high and low miPRS in the training cohort (n=208). (f) Partial results of immune cells infiltration evaluation between high and low miPRS in the validation cohort (n=154). (g) Radar chart to evaluate infiltration of 22 types of immune cells between high and low miPRS in the validation cohort (n=154).

Generally, these studies verified the rationality and accuracy the miPRS.

Signature reassessment combined with other clinical variates

In order to better translate our signature into clinical application, we used multivariate Cox proportional hazards regression analysis to reassess the signature by combining miPRS and other clinical variates including age, cancer grade, and stage (Fig. 9a). Kaplan-Meier survival analysis illustrated significant difference of prognosis between high and low risk group stratified by the signature combined with clinical variates both in the training and validation cohort (Fig. 9b, d). Furthermore, to evaluate the combined signature, time-dependent ROC curve was performed, and the Area Under Curve (AUC) of the 1-, 5-, and 10-year presented 0.92, 0.84 and 0.82 in the training cohort and 0.76, 0.74 and 0.72 in the validation cohort, higher than using miPRS signature only (Figs. 9c, e, 2e, h). Nomogram was employed to visualize the modified signature, in which all variates involved in the signature were quantified. Higher ages, grades, stages, and miPRSs contributed to lower total points, leading to poorer prognosis (Fig. 9f). Furthermore, the calibration curve demonstrated that when the actual survival rate was less than 20% or more than 80%, the signature tended to overestimate the risk while when survival rate was between 20% and 80% the conclusion was the opposite (Fig. 9g).

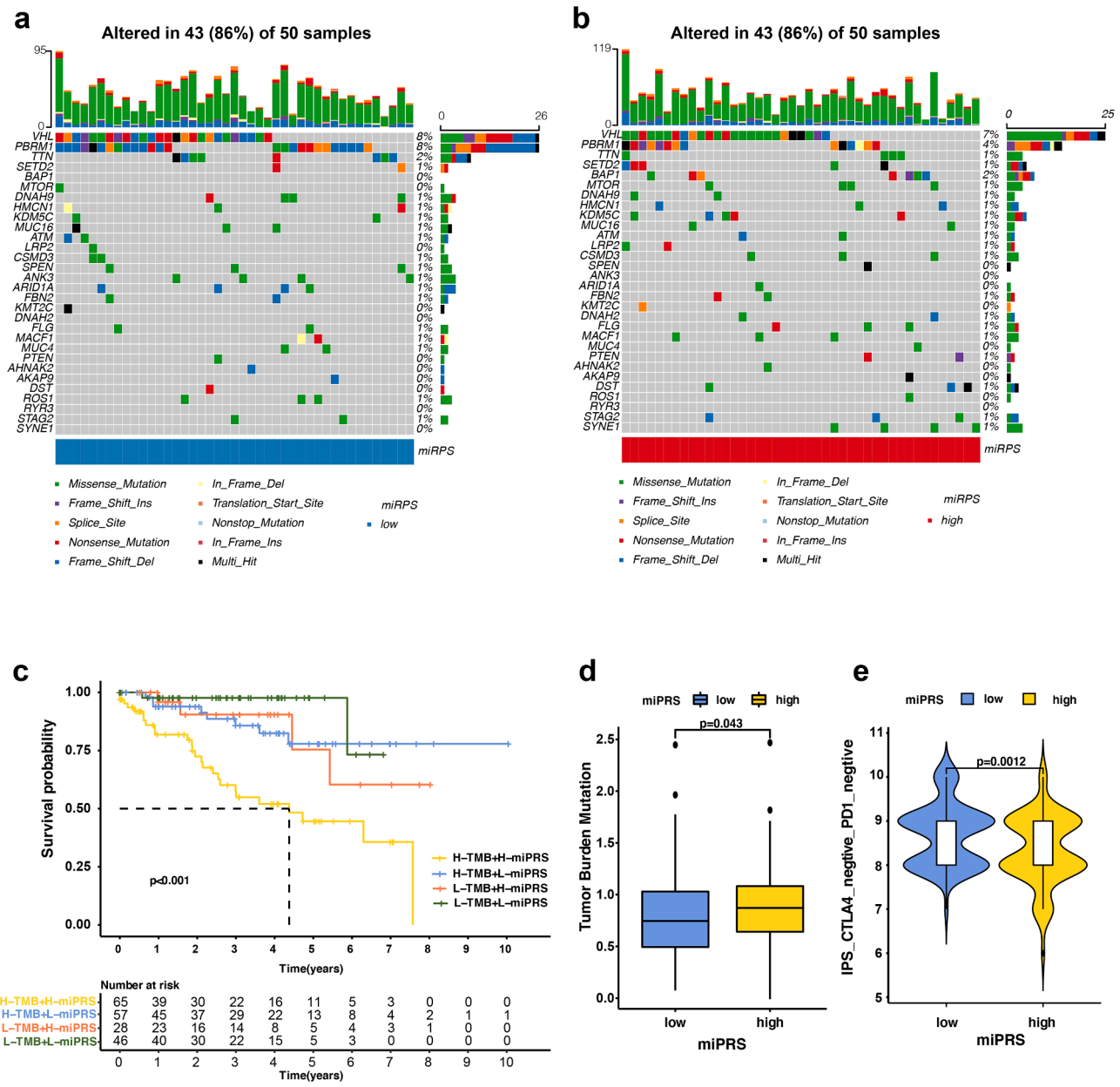

Fig. 5. Tumor Mutation Burden (TMB) analysis and immunophenoscore (IPS) analysis. (a) Heatmap of TMB of low miPRS (n=50). (b) Heatmap of TMB of high miPRS (n=50). (c) Kaplan-Meier survival analysis of TMB combined with miPRS in the training cohort (n=196). (d) TMB contrast between low and high miPRS (n=196). (e) IPS analysis between low and high miPRS in the training cohort (n=152).

Discussion

MicroRNAs (miRNAs) are small non-coding RNA with 18-24 nucleotides, which can act as regulators of mRNAs to perform multiple regulatory functions and are involved in various biological processes in the occurrence and metastasis of tumors [56,57]. Due to the significant biological functions of miRNA, more and more research demonstrated that miRNAs are effective prognostic markers for ccRCC. The aberrant expression of miR221 and miR32 can predict the mortality and the downregulation of miR-30a-5p is an indicator of metastatic dissemination as well as worse survival in ccRCC [58,59]. Recently, multiple prediction models utilizing miRNA have been published [60–62]. However, due to the discrepancy of sequencing platform and analyzing process, these models based on relatively-absolute quantity of miRNAs are not qualified to assess data from other studies.

In this study, we introduced an evaluation system miPRS based on the comparison within miRNA pairs to predict the the survival of ccRCC for the first time in the world. This algorithm has better compatibility with data from different studies when analyzed with other conventional models. Our data demonstrated miPRS achieved impressive potency and was proven to be an independent coefficient in survival prediction within all training, validation, and testing cohorts (Fig. 2). Other than distinct survival status, patient groups with different miPRS also showed different intrinsic molecular characteristics. Additionally, the miPRS signature was also a prognostic factor independent from other clinical variates (Fig. 3).

Transcriptional analysis revealed that low-miPRS group seemed to be immunocompetent individuals while patients with high-miPRS were immunocompromised. In low-risk group, more GO features concerning antigen presentation like antigen binding and immunoglobin complex were enriched (Fig. 4). However, activated dendritic cells (DCs) in both groups were low and there were even more resting DCs found in low-risk

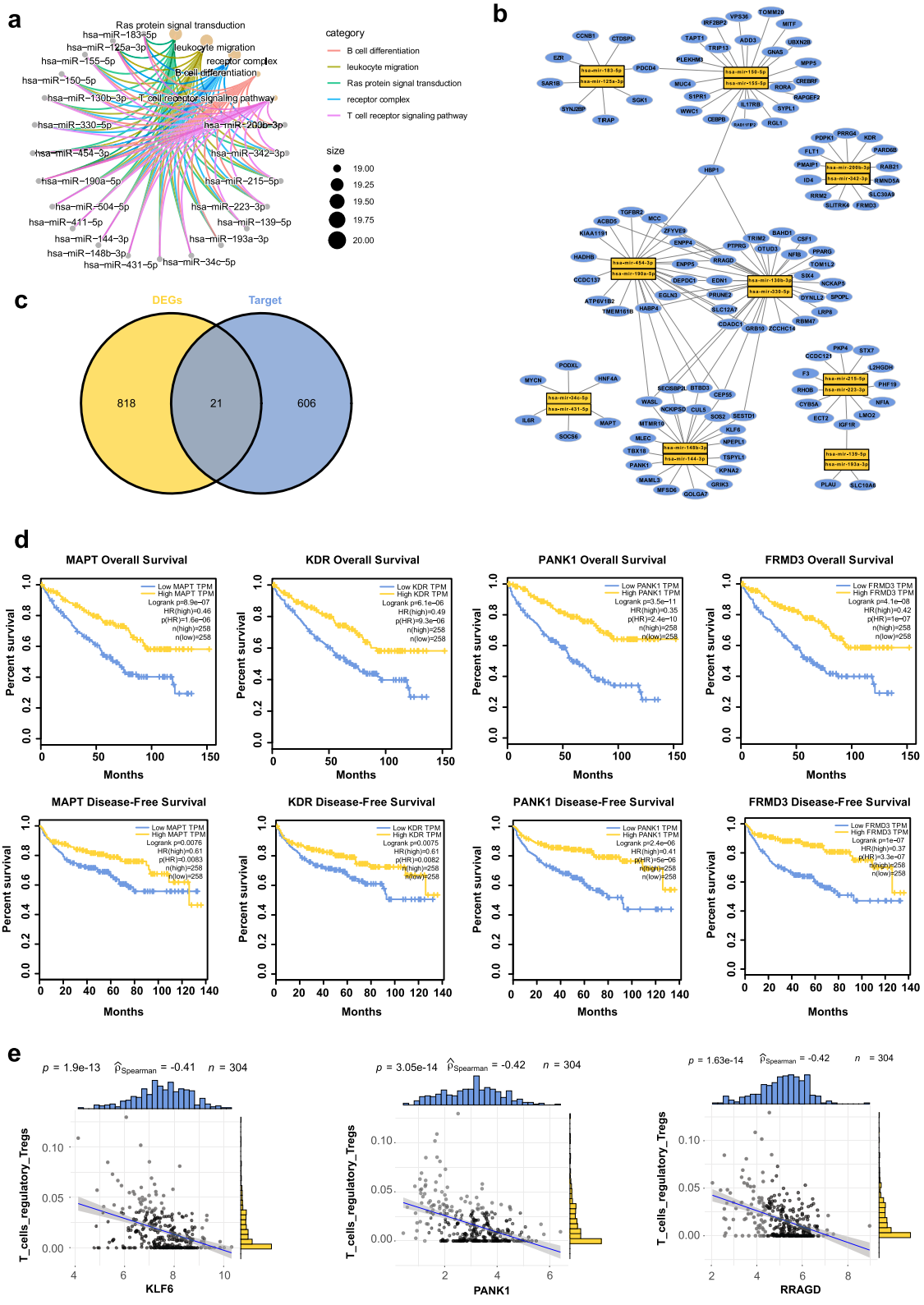

Fig. 6. miRNA enrichment analysis and prediction and analysis of target genes of the miRNA signature. (a) Enrichment analysis of miRNA from the signature. (b) Network of target genes predicted from the miRNA signature. Differentially Expressed Gene (DEG) analysis between high and low miPRS in the training cohort (n=150). (c) Venn gram of DEGs and target genes. (d) OS and DFS Kaplan-Meier survival analysis (n=516) of partial survival related genes shared by DEGs and target genes. (e) Correlation profile (n=304) of T cells regulatory (Tregs) and survival related genes shared by DEGs and target genes. OS, Overall Survival; DFS, Disease-Free Survival.

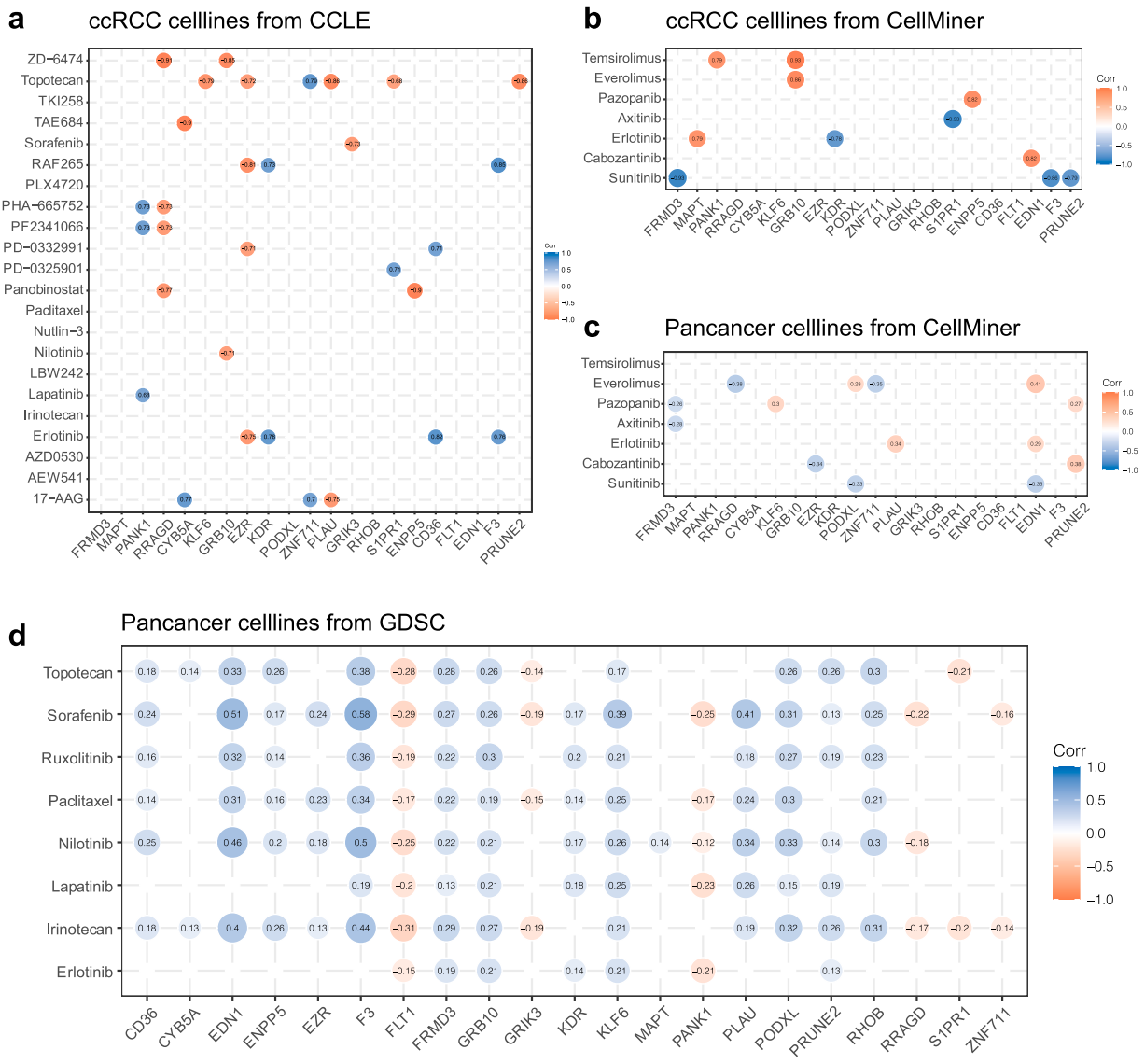

Fig. 7. Drug sensitivity analysis. (a) Heatmap of correlation coefficient profile between 21 genes and 22 types of drugs in ccRCC cell lines from CCLE. (b) Heatmap of correlation coefficient profile between 21 genes and 7 types of drugs in ccRCC cell lines from NCI-60 on CellMiner. (c) Heatmap of correlation coefficient profile between 21 genes and 7 types of drugs in pan-cancer cell lines from NCI-60 on CellMiner. (d) Heatmap of correlation coefficient profile between 21 genes and 8 types of drugs in pan-cancer cell lines from GDSC.

group, indicating that the antigen presenting process within low-risk group was disturbed due to inept DCs [63]. As for high-miPRS group, there were far more Tregs within, correspondingly to the finding that there were less CTLA4- PD-1- IPS in high-risk group [64]. These results suggest two completely different treatment directions for low- and high-risk groups. Patients with the low miPRS might be good candidates for further study of DC-based immune therapy [27]. High-miPRS patients are more likely to benefit from immune checkpoint blockers or other therapies attempting to bypass the negative regulation of Tregs [64].

The difference between two groups was also reflected in genomic mutation. Though roughly analogous in genes mutated in two groups, low-miPRS group showed much higher frame shift mutation rate in the most commonly mutated genes VHL, and higher total mutation rate of PBRM1 (Fig. 5). VHL gene inactivation is the most common cancer driving event in ccRCC [65]. In low-miPRS group, more frame shift mutation might correspond with more impact on the structure and thus function of VHL. Low-miPRS group tends to acquire ccRCC at a younger age (p=0.107). PBRM1 is a subunit of the PBAF chromatin remodeling complex [66]. Its deficiency was discovered to display synthetic lethality with application of DNA repair inhibitors like PARPi and ATRi [67]. High-miPRS group also had higher TMB. Further, when we split each group according to their TMB respectively to create four new groups, survival analysis showed significant discrepancy among 4 groups, with high-miPRS-high-TMB showing worst survival. Higher TMB has been found to be related with better response to immune therapy like ICBs, corresponding to our result derived from transcriptional level analysis [68].

Next, the enrichment of miRNA showed that 20 miRNAs consisting miPRS mainly involved immune related biological processes like leukocyte migration, B cell differentiation, etc. Within 21 common genes of DEGs between two risk groups and downstream of 20 miRNAs, 4 genes (MAPT, KDR, PANK1, FRMD3) are found significantly related with both OS and PFS and 3 genes (KLF6, PANK1, RRAGD) were correlated with infiltration of Tregs (Fig. 6). MAPT, or microtubule associated protein tau, has been reported to as promising biomarkers for the prediction of ccRCC, and knock-down of MAPT was found to increase proliferation and invasion of ccRCC cells [69,70]. KDR or

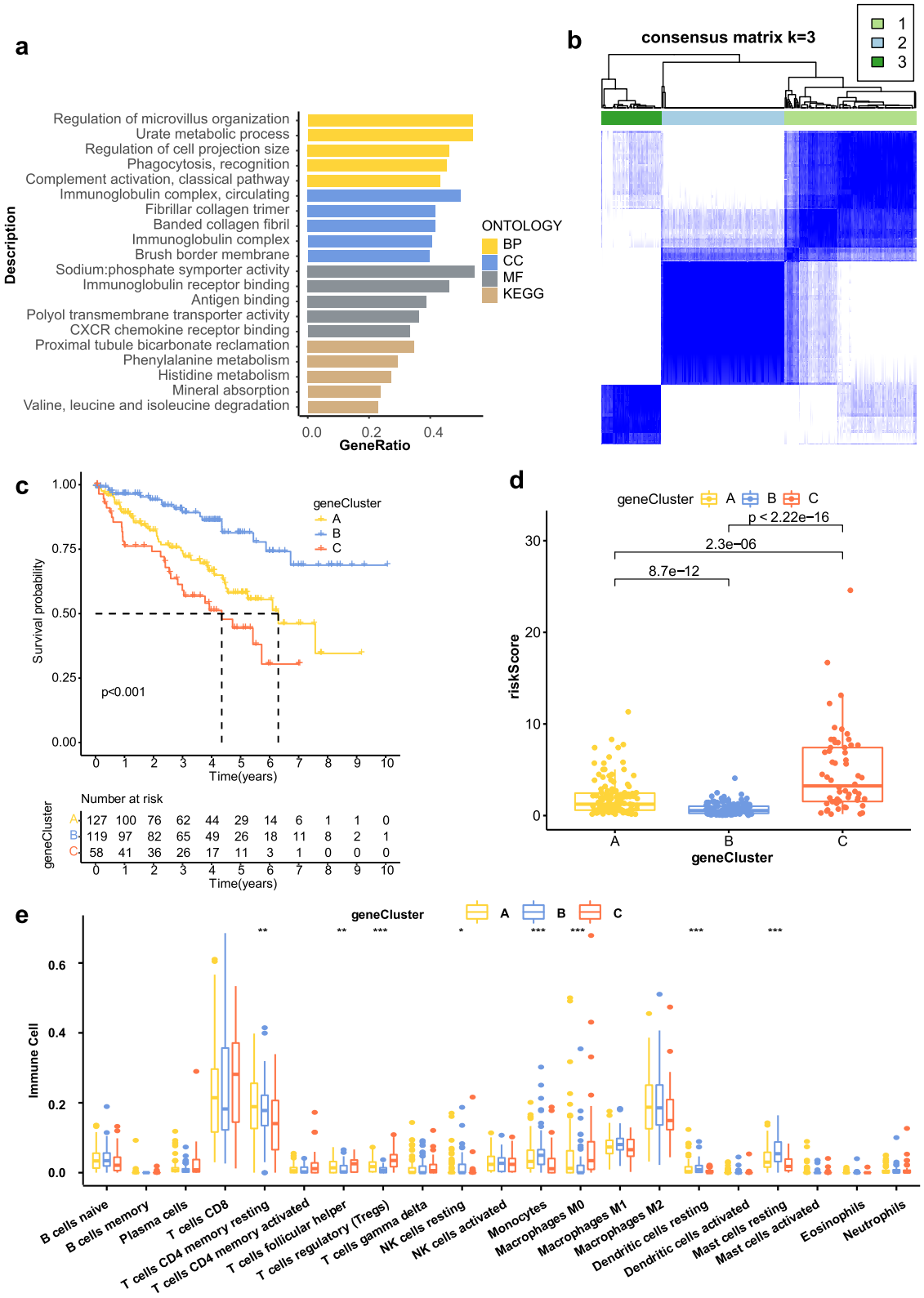

Fig. 8. DEGs functional enrichment and clustering analysis. (a) Functional enrichment of DEGs between high and low miPRS in the training cohort (n=150) from the respective of biological process, molecular function, cellular component and Kyoto Encyclopedia of Genes and Genomes (KEGG) analysis. (b) DEG clustering analysis in the training cohort (n=304). (c) Kaplan-Meier survival analysis of training cohort (n=304) stratified by the gene clusters. (d) Contrast of miPRS between individuals from different gene clusters in the training cohort (n=304). (e) Evaluation of 22 immune cells infiltration between different gene clusters in the training cohort (n=208).

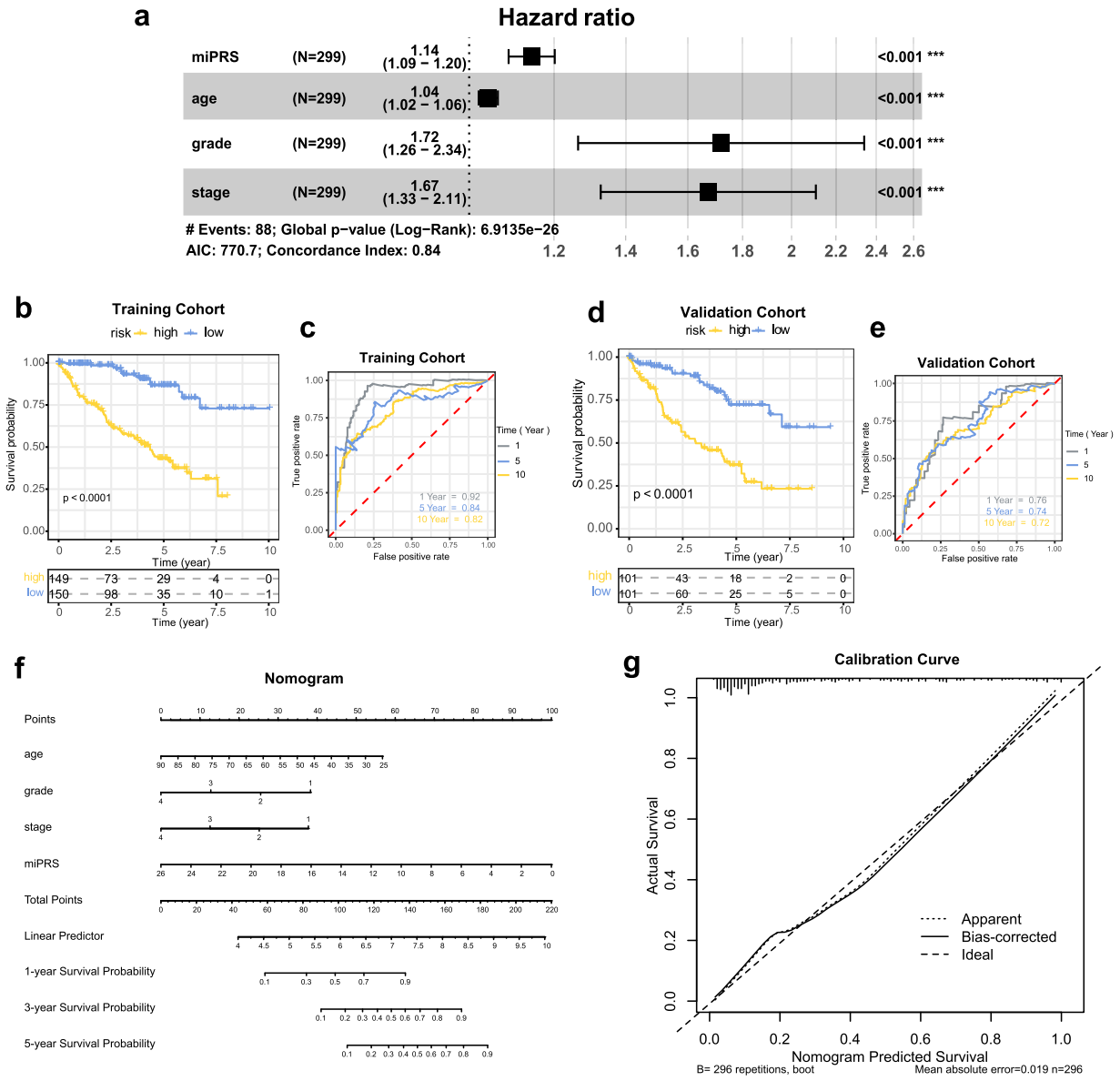

Fig. 9. Signature reassessment combined with other vital clinical characteristics. (a) Multivariate Cox proportional hazards regression analysis of miPRS, age, grade and stage. (b) Kaplan-Meier survival analysis of training cohort (n=299) stratified by median of risk score. (c) Time-dependent ROC curve of the training cohort (n=299). (d) Kaplan-Meier survival analysis of validation cohort (n=202). (e) Time-dependent ROC curve of the training cohort (n=202) to evaluate the signature. (f) Nomogram of the miPRS combined with other clinical characteristics. (g) Calibration Curve of the combined model.

VEGFR2 were negatively correlated with survival of ccRCC [71] and multiple chemicals and mAbs have been proposed as promising treatments in KDR altered patients [72–74]. PANK1 codes isotypes of pantothenate kinase associated neurodegeneration, of which the intron 5 encodes a highly conserved microRNA. miR107 has been reported as an a tumor suppressor previously, analogous to finding to this article [75]. FRMD3 (4.1 protein ezrin, radixin, moesin [FERM] domain containing 3) was broadly considered associated with diabetic nephropathy by genome wide association studies (GWAS) [76,77], but no publications have revealed its potential role in the pathogenesis of ccRCC, and deserves further research. KLF6 is a protective transcription factor in ccRCC that suppresses metastasis of ccRCC by activation of E2F1 [78]. However, activation of E2F1 was reported to increase CD39 and CD73 on the surface Treg, leading to intensified Treg functions in hypoxic TME [79,80]. RRAGD, which has been identified as a tumor growth-promoting factor, is elevated when anti-oncogene FLCN (germline mutations in the Folliculin) is mutated through the activation of TFE3/TFEB [81]. In the meanwhile, TFE3/TFEB could upregulate cytokines leading pathogen resistance [82].

Fig. 7 shows the drug sensitivity analysis of ccRCC to various antitumor drugs. Previous studies have shown that sunitinib (a vascular endothelial growth factor receptor (VEGFR)-targeting biologic) is more potent than topotecan (a topoisomerase 1 toxicant and hypoxia-inducible factors 1α and 2α (HIFs) synthetic inhibitors) with stronger tumor-suppressive activity [83]. Another study claimed that when methylselenocysteine (MSC) was combined with sunitinib, topotecan, and S-1 (a 5-fluorouracil prodrug) durable drug responses would be obtained [84]. This synergy was proved to be associated with enhanced tumor vasculature stability, downregulation of 28 oncogenic miRNAs, and upregulation of 12 tumor suppressor miRNAs [85].

In DEG cluster analysis, we found that the high abundance of macrophages M0 in class B shortened the overall survival of ccRCC patients, and the opposite was true in class A. Previous studies have demonstrated that immunosuppressive cells, such as M0 macrophages, are higher in high-risk ccRCC patients, while the proportion of active immune cells, including naive B cells, resting CD4 memory T cells, resting natural killer

(NK) cells were lower, indicating the presence of an immunosuppressive microenvironment [86,87].

Finally, we reconstructed a more clinically useful model using miPRS, age, gender, and stage, the four independent prognostic indicators, and displayed the Nomogram. For each ccRCC patient, the corresponding risk score can be calculated through the four variables of miRPS, age, gender and tumor stage, and its corresponding 1-year, 3-year and 5-year survival probability can be found intuitively in the Nomogram. Furthermore, the robust performance of the model, compared with traditional clinical factors, shows a strong potential for clinical application. The predictive models based on miPRS and other clinical factors could serve as a promising tool for stratifying patients, thereby facilitating future ccRCC treatments.

Although the performance of the model is very robust and stable, there are still some limitations that we cannot avoid in the present study. First, the biological mechanism of how the 20 miRNAs involved in the signature to regulate the occurrence and development of diseases remains unanswered. Second, the disease progression-related pathways obtained by enrichment analysis still await evidence and interpretation from more omic data. Third, although most of the information is still retained, some miRNAs are inevitably lost when conducting intersection due to differences in the total number and nomenclature of miRNAs in various platforms. We are looking forward to witnessing the emergence of more unified and standardized miRNA platforms in the future.

Conclusion

In this study, we constructed and validated a high-potency prediction signature based on 10 miRNA pairs for ccRCC. Genomic, transcriptional and immune infiltration characteristics in patients with high or low miPRS were revealed, as well as tumor immune microenvironment and tumor immunogenicity, to clarify the significance of this prediction signature. Additionally, we also proposed potential therapeutic targets and agents for ccRCC with the signature by integrating multi-omics data. This study of the innovative miRNA signature sheds light on the prediction and treatment of ccRCC to improve prognosis.

Data availability statement

All data can be obtained from TCGA (https://portal.gdc.cancer.gov/) and GEO (https://www.ncbi.nlm.nih.gov/geo/) database. Other queries for data and code could be directly sent to the corresponding author.

Funding

This study was supported by research grants from the China National Natural Scientific Foundation (81903972, 82002018, and 82170752) and Shanghai Sailing Program (19YF1406700 and 20YF1406000). The funders had no roles in study design, data collection and analysis, decision to publish, or preparation of the manuscript.

Data sharing

All data included in this study is retrieved from open source database.

Authors' contributions

Wang Yulin provided the original idea of the paper, analyzed the data and wrote the draft of the manuscript. Shen Ziyan reviewed and revised the manuscript. Mo Shaocong, Dai Leijie, Song Biao, and Gu Wenchao designed the study, debugged the code and guided the analysis. Yu Xixi, Zhang Han and Chen Jing served as scientific advisors and supervised data analysis. Gu Yulu, Lv Shiqi, Zhang Di and Yu Xixi polished the article. Zhang Xiaoyan and Ding Xiaoqiang were co-investigators and supervisors of the study. All authors contributed to the article and approved the submitted version.

Declaration of Competing Interest

There are no conflicts of interests to declare.

Acknowledgment

We would like thank Dr. Linxi Zhao for his proofreading of this manuscript.

Supplementary materials

Supplementary material associated with this article can be found, in the online version, at doi:10.1016/j.tranon.2022.101519.

References

[1] U. Capitanio, K. Bensalah, A. Bex, S. Boorjian, F. Bray, J. Coleman, et al., Epidemiology of renal cell carcinoma, Eur. Urol. 75 (1) (2019) 74–84.
[2] V. Miranda-Gonçalves, A. Lameirinhas, R. Henrique, F. Baltazar, C. Jerónimo, The metabolic landscape of urological cancers: new therapeutic perspectives, Cancer Lett. 477 (2020) 76–87.
[3] Publication N. SEER cancer statistics review. 2015.
[4] K. Trpkov, O. Hes, S.R. Williamson, A.J. Adeniran, A. Agaimy, R. Alaghehbandan, et al., New developments in existing WHO entities and evolving molecular concepts: the genitourinary pathology society (GUPS) update on renal neoplasia, Mod. Pathol. 34 (7) (2021) 1392–1424.
[5] J. Angulo, C. Manini, J. López, A. Pueyo, B. Colás, S. Ropero, The role of epigenetics in the progression of clear cell renal cell carcinoma and the basis for future epigenetic treatments, Cancers 13 (9) (2021).
[6] R.D. Arora, F. Limaiem, Renal clear cell cancer. StatPearls. StatPearls Publishing Copyright © 2021, StatPearls Publishing LLC, Treasure IslandFL, 2021.
[7] L. Albiges, T. Powles, M. Staehler, K. Bensalah, R. Giles, M. Hora, et al., Updated european association of urology guidelines on renal cell carcinoma: immune checkpoint inhibition is the new backbone in first-line treatment of metastatic clear-cell renal cell carcinoma, Eur. Urol. 76 (2) (2019) 151–156.
[8] E. Lin, X. Liu, Y. Liu, Z. Zhang, L. Xie, K. Tian, et al., Roles of the dynamic tumor immune microenvironment in the individualized treatment of advanced clear cell renal cell carcinoma, Front. Immunol. 12 (2021), 653358.
[9] B.R. Christensen, Y.M. Hajja, V. Koshkin, PC. Barata, Update on first-line combination treatment approaches in metastatic clear-cell renal cell carcinoma, Curr. Treat. Opt. Oncol. 22 (2) (2021) 15.
[10] V. Loo, M. Salgia, P. Bergerot, E.J. Philip, SK. Pal, First-line systemic therapy for metastatic clear-cell renal cell carcinoma: critical appraisal of emerging options, Target. Oncol. 14 (6) (2019) 639–645.
[11] J. Graham, B. Bhindi, D.Y.C. Heng, The evolving role of cytoreductive nephrectomy in metastatic renal cell carcinoma, Curr. Opin. Urol. 29 (5) (2019) 507–512.
[12] A.A. Lalani, B.A. McGregor, L. Albiges, T.K. Choueiri, R. Motzer, T. Powles, et al., Systemic treatment of metastatic clear cell renal cell carcinoma in 2018: current paradigms, use of immunotherapy, and future directions, Eur. Urol. 75 (1) (2019) 100–110.
[13] B. Delahunt, J.N. Eble, H. Samaratunga, M. Thunders, J.W. Yaxley, L. Egevad, Staging of renal cell carcinoma: current progress and potential advances, Pathology 53 (1) (2021) 120–128.
[14] K. Taneja, S.R. Williamson, Updates in pathologic staging and histologic grading of renal cell carcinoma, Surg. Pathol. Clin. 11 (4) (2018) 797–812.
[15] C. Qin, L.J. Sun, L. Cui, Q. Cao, J. Zhu, P. Li, et al., Application of the revised Tumour Node Metastasis (TNM) staging system of clear cell renal cell carcinoma in eastern China: advantages and limitations, Asian J. Androl. 15 (4) (2013) 550–557.
[16] A. Volpe, J.J. Patard, Prognostic factors in renal cell carcinoma, World J. Urol. 28 (3) (2010) 319–327.
[17] A. Galfano, G. Novara, M. Iafrate, S. Cavalleri, G. Martignoni, M. Gardiman, et al., Mathematical models for prognostic prediction in patients with renal cell carcinoma, Urol. Int. 80 (2) (2008) 113–123.
[18] S. Ghafouri-Fard, Z. Shirvani-Farsani, W. Branicki, M. Taheri, MicroRNA Signature in renal cell carcinoma, Front. Oncol. 10 (2020), 596359.
[19] A. Schaefer, C. Stephan, J. Busch, G. Yousef, K. Jung, Diagnostic, prognostic and therapeutic implications of microRNAs in urologic tumors, Nat. Rev. Urol. 7 (5) (2010) 286–297.
[20] J. Oto, E. Plana, J.V. Sánchez-González, J. García-Olaverri, Á. Fernández-Pardo, F. España, et al., Urinary microRNAs: looking for a new tool in diagnosis, prognosis, and monitoring of renal cancer, Curr. Urol. Rep. 21 (2) (2020) 11.
[21] L. Kinget, E. Roussel, D. Lambrechts, B. Boeckx, L. Vanginderhuysen, M. Albersen, et al., MicroRNAs possibly involved in the development of bone metastasis in clear-cell renal cell carcinoma, Cancers 13 (7) (2021).
[22] Y.H. He, C. Chen, Z. Shi, The biological roles and clinical implications of microRNAs in clear cell renal cell carcinoma, J. Cell. Physiol. 233 (6) (2018) 4458–4465.

[23] L. Ran, J. Liang, X. Deng, J. Wu, miRNAs in prediction of prognosis in clear cell renal cell carcinoma, BioMed Res. Int. 2017 (2017), 4832931.
[24] Y. Xiong, Y. Qi, W. Lin, Q. Bai, L. Liu, J. Guo, Development and validation of an individualized DNA repair-related gene signature in localized clear cell renal cell carcinoma, World J. Urol. 39 (4) (2021) 1203–1210.
[25] H. Nie, F. Bu, J. Xu, T. Li, J. Huang, 29 immune-related genes pairs signature predict the prognosis of cervical cancer patients, Sci. Rep. 10 (1) (2020) 14152.
[26] X. Jiang, Y. Gao, N. Zhang, C. Yuan, Y. Luo, W. Sun, et al., Establishment of immune-related gene pair signature to predict lung adenocarcinoma prognosis, Cell Transplant. 29 (2020), 963689720977131.
[27] J. Zhou, Y. Yi, C. Wang, C. Su, Y. Luo, Identification of a 3-mRNA signature as a novel potential prognostic biomarker in patients with ovarian serous cystadenocarcinoma in G2 and G3, Oncol. Lett. 18 (4) (2019) 3545–3552.
[28] F. Zhang, Y. Liu, Y. Yang, K. Yang, Development and validation of a fourteen-innate immunity-related gene pairs signature for predicting prognosis head and neck squamous cell carcinoma, BMC Cancer 20 (1) (2020) 1015.
[29] M.J. Moynihan, T.B. Sullivan, E. Burks, J. Schober, M. Calabrese, A. Fredrick, et al., MicroRNA profile in stage I clear cell renal cell carcinoma predicts progression to metastatic disease, Urol. Oncol. 38 (10) (2020) 799, e11- e22.
[30] S. Griffiths-Jones, R.J. Grocock, S. van Dongen, A. Bateman, AJ. Enright, miRBase: microRNA sequences, targets and gene nomenclature, Nucleic Acids Res. 34 (Database issue) (2006) D140–D144.
[31] C. Gene Ontology, Gene ontology consortium: going forward, Nucleic. Acids. Res. 43 (Database issue) (2015) D1049–D1056.
[32] H. Ogata, S. Goto, K. Sato, W. Fujibuchi, H. Bono, M. Kanehisa, KEGG: Kyoto encyclopedia of genes and genomes, Nucleic Acids Res. 27 (1) (1999) 29–34.
[33] A. Subramanian, P. Tamayo, V.K. Mootha, S. Mukherjee, B.L. Ebert, M.A. Gillette, et al., Gene set enrichment analysis: a knowledge-based approach for interpreting genome-wide expression profiles, Proc. Natl. Acad. Sci. U. S. A. 102 (43) (2005) 15545–15550.
[34] G. Yu, L.G. Wang, Y. Han, Q.Y. He, clusterProfiler: an R package for comparing biological themes among gene clusters, OMICS 16 (5) (2012) 284–287.
[35] F. Kern, T. Fehlmann, J. Solomon, L. Schwed, N. Grammes, C. Backes, et al., miEAA 2.0: integrating multi-species microRNA enrichment analysis and workflow management systems, Nucleic Acids Res. 48 (W1) (2020) W521–W5W8.
[36] B. Chen, M.S. Khodadoust, C.L. Liu, A.M. Newman, A.A. Alizadeh, Profiling tumor infiltrating immune cells with CIBERSORT, Methods Mol. Biol. 1711 (2018) 243–259.
[37] A. Mayakonda, D.C. Lin, Y. Assenov, C. Plass, H.P. Koeffler, Maftools: efficient and comprehensive analysis of somatic variants in cancer, Genome Res. 28 (11) (2018) 1747–1756.
[38] Y. Chen, X. Wang, miRDB: an online database for prediction of functional microRNA targets, Nucleic Acids Res. 48 (D1) (2020) D127–DD31.
[39] S.D. Hsu, F.M. Lin, W.Y. Wu, C. Liang, W.C. Huang, W.L. Chan, et al., miRTarBase: a database curates experimentally validated microRNA-target interactions, Nucleic Acids Res. 39 (Database issue) (2011) D163–D169.
[40] V. Agarwal, G.W. Bell, J.W. Nam, D.P. Bartel, Predicting effective microRNA target sites in mammalian mRNAs, Elife 4 (2015).
[41] P. Shannon, A. Markiel, O. Ozier, N.S. Baliga, J.T. Wang, D. Ramage, et al., Cytoscape: a software environment for integrated models of biomolecular interaction networks, Genome Res. 13 (11) (2003) 2498–2504.
[42] M.E. Ritchie, B. Phipson, D. Wu, Y. Hu, C.W. Law, W. Shi, et al., limma powers differential expression analyses for RNA-sequencing and microarray studies, Nucleic Acids Res. 43 (7) (2015) e47.
[43] M.D. Wilkerson, D.N. Hayes, ConsensusClusterPlus: a class discovery tool with confidence assessments and item tracking, Bioinformatics 26 (12) (2010) 1572–1573.
[44] A. Luna, F. Elloumi, S. Varma, Y. Wang, V.N. Rajapakse, M.I. Aladjem, et al., CellMiner Cross-Database (CellMinerCDB) version 1.2: exploration of patient-derived cancer cell line pharmacogenomics, Nucleic Acids Res. 49 (D1) (2021) D1083–D1D93.
[45] W. Yang, J. Soares, P. Greninger, E.J. Edelman, H. Lightfoot, S. Forbes, et al., Genomics of Drug Sensitivity in Cancer (GDSC): a resource for therapeutic biomarker discovery in cancer cells, Nucleic Acids Res. 41 (Database issue) (2013) D955–D961.
[46] M. Ghandi, F.W. Huang, J. Jane-Valbuena, G.V. Kryukov, C.C. Lo, E. R. McDonald 3rd, et al., Next-generation characterization of the cancer cell line encyclopedia, Nature 569 (7757) (2019) 503–508.
[47] W.C. Reinhold, M. Sunshine, S. Varma, J.H. Doroshow, Y. Pommier, Using CellMiner 1.6 for systems pharmacology and genomic analysis of the NCI-60, Clin. Cancer Res. 21 (17) (2015) 3841–3852.
[48] W.C. Reinhold, M. Sunshine, H. Liu, S. Varma, K.W. Kohn, J. Morris, et al., CellMiner: a web-based suite of genomic and pharmacologic tools to explore transcript and drug patterns in the NCI-60 cell line set, Cancer Res. 72 (14) (2012) 3499–3511.
[49] N.R. Rydzewski, E. Peterson, J.M. Lang, M. Yu, S. Laura Chang, M. Sjostrom, et al., Predicting cancer drug TARGETS - TreAtment Response Generalized Elastic-neT Signatures, NPJ Genom. Med. 6 (1) (2021) 76.
[50] J. Barretina, G. Caponigro, N. Stransky, K. Venkatesan, A.A. Margolin, S. Kim, et al., The cancer cell line encyclopedia enables predictive modelling of anticancer drug sensitivity, Nature 483 (7391) (2012) 603–607.
[51] J. Barretina, G. Caponigro, N. Stransky, K. Venkatesan, A.A. Margolin, S. Kim, et al., Addendum: the cancer cell line encyclopedia enables predictive modelling of anticancer drug sensitivity, Nature 565 (7738) (2019) E5–E6.
[52] Z. Wan, X. Zhang, Y. Luo, B. Zhao, Identification of hepatocellular carcinoma-related potential genes and pathways through bioinformatic-based analyses, Genet. Test Mol. Biomark. 23 (11) (2019) 766–777.
[53] A. Iasonos, D. Schrag, G.V. Raj, K.S. Panageas, How to build and interpret a nomogram for cancer prognosis, J. Clin. Oncol. 26 (8) (2008) 1364–1370.
[54] B. Van Calster, D.J. McLernon, M. van Smeden, L. Wynants, E.W. Steyerberg, Evaluating diagnostic t, et al. Calibration: the Achilles heel of predictive analytics, BMC Med. 17 (1) (2019) 230.
[55] Z. Tang, C. Li, B. Kang, G. Gao, C. Li, Z. Zhang, GEPIA: a web server for cancer and normal gene expression profiling and interactive analyses, Nucleic Acids Res. 45 (W1) (2017) W98–W102.
[56] G. Romano, M. Acunzo, Nana-Sinkam P. microRNAs as Novel Therapeutics in Cancer, Cancers 13 (7) (2021).
[57] A. Schaefer, M. Jung, G. Kristiansen, M. Lein, M. Schrader, K. Miller, et al., MicroRNAs and cancer: current state and future perspectives in urologic oncology, Urol. Oncol. 28 (1) (2010) 4–13.
[58] A.L. Teixeira, M. Ferreira, J. Silva, M. Gomes, F. Dias, J.I. Santos, et al., Higher circulating expression levels of miR-221 associated with poor overall survival in renal cell carcinoma patients, Tumour Biol. 35 (5) (2014) 4057–4066.
[59] D. Petillo, E.J. Kort, J. Anema, K.A. Furge, X.J. Yang, B.T. Teh, MicroRNA profiling of human kidney cancer subtypes, Int. J. Oncol. 35 (1) (2009) 109–114.
[60] X. Wang, L. Han, L. Zhou, L. Wang, L.M. Zhang, Prediction of candidate RNA signatures for recurrent ovarian cancer prognosis by the construction of an integrated competing endogenous RNA network, Oncol. Rep. 40 (5) (2018) 2659–2673.
[61] O.D. Tavabie, C.J. Karvellas, S. Salehi, J.L. Speiser, C.F. Rose, K. Menon, et al., A novel microRNA-based prognostic model outperforms standard prognostic models in patients with acetaminophen-induced acute liver failure, J. Hepatol. (2021).
[62] J. Wen, K. Luo, H. Liu, S. Liu, G. Lin, Y. Hu, et al., MiRNA Expression analysis of pretreatment biopsies predicts the pathological response of esophageal squamous cell carcinomas to neoadjuvant chemoradiotherapy, Ann. Surg. 263 (5) (2016) 942–948.
[63] O.V. Kovaleva, D.V. Samoilova, M.S. Shitova, A. Gratchev, Tumor associated macrophages in kidney cancer, Anal. Cell. Pathol. (Amsterdam) 2016 (2016), 9307549.
[64] P.M. Rappold, A.W. Silagy, R.R. Kotecha, A.A. Hakimi, Immune checkpoint blockade in renal cell carcinoma, J. Surg. Oncol. 123 (3) (2021) 739–750.
[65] W. Yang, J. Zhou, K. Zhang, L. Li, Y. Xu, K. Ma, et al., Identification and validation of the clinical roles of the VHL-related LncRNAs in clear cell renal cell carcinoma, J. Cancer 12 (9) (2021) 2702–2714.
[66] M. Karki, R.K. Jangid, R. Anish, R.N.H. Seervai, J.P. Bertocchio, T. Hotta, et al., A cytoskeletal function for PBRM1 reading methylated microtubules, Sci. Adv. 7 (14) (2021).
[67] R.M. Chabanon, D. Morel, T. Eychenne, L. Colmet-Daage, I. Bajrami, N. Dorvault, et al., PBRM1 Deficiency confers synthetic lethality to DNA repair inhibitors in cancer, Cancer Res. (2021).
[68] T.A. Chan, M. Yarchoan, E. Jaffee, C. Swanton, S.A. Quezada, A. Stenzinger, et al., Development of tumor mutation burden as an immunotherapy biomarker: utility for the oncology clinic, Ann. Oncol. 30 (1) (2019) 44–56.
[69] X. Han, Y. Sekino, T. Babasaki, K. Goto, S. Inoue, T. Hayashi, et al., Microtubule-associated protein tau (MAPT) is a promising independent prognostic marker and tumor suppressive protein in clear cell renal cell carcinoma, Urol. Oncol. 38 (6) (2020) 605, e9-.e17.
[70] Y. Sun, J. Zou, W. Ouyang, K. Chen, Identification of PDE7B as a potential core gene involved in the metastasis of clear cell renal cell carcinoma, Cancer Manag. Res. 12 (2020) 5701–5712.
[71] M. Volkova, I. Tsimafeyeu, A. Olshanskaya, Y. Khochenkova, E. Solomko, S. Ashuba, et al., Expression of growth factors and their receptors in the primary renal cell carcinoma: new data and review, Cent. Eur. J. Urol. 73 (4) (2020) 466–475.
[72] N. Wei, J. Liang, S. Peng, Q. Sun, Q. Dai, M. Dong, Design, synthesis, and biological evaluation of Axitinib derivatives, Molecules (Basel, Switzerland) 23 (4) (2018).
[73] K. Sharma, K. Patidar, M.A. Ali, P. Patil, H. Goud, T. Hussain, et al., Structure-based virtual screening for the identification of high affinity compounds as potent VEGFR2 inhibitors for the treatment of renal cell carcinoma, Curr. Top. Med. Chem. 18 (25) (2018) 2174–2185.
[74] G.C. Cabozantinib, Multi-kinase inhibitor of MET, AXL, RET, and VEGFR2, Recent Results Cancer Res. 211 (2018) 67–75.
[75] Z. Luo, Y. Zheng, W. Zhang, Pleiotropic functions of miR107 in cancer networks, Oncol. Targets Ther. 11 (2018) 4113–4124.
[76] S. Al-waheeb, M. Alwohhaib, A. Abdelghani, S. Al-Sharrah, E. Al-Shafey, A. Al-Sahow, et al., Evaluation of associations between single nucleotide polymorphisms in the FRMD3 and CARS genes and diabetic nephropathy in a Kuwaiti population, Genet. Mol. Res. 15 (1) (2016).
[77] M.P. Buffon, D.A. Sortica, F. Gerchman, D. Crispim, L.H. Canani, FRMD3 gene: its role in diabetic kidney disease. A narrative review, Diabetol. Metab. Syndr. 7 (2015) 118.
[78] Y. Gao, H. Li, X. Ma, Y. Fan, D. Ni, Y. Zhang, et al., KLF6 Suppresses metastasis of clear cell renal cell carcinoma via transcriptional repression of E2F1, Cancer Res. 77 (2) (2017) 330–342.
[79] R. Bao, X. Shui, J. Hou, J. Li, X. Deng, X. Zhu, et al., Adenosine and the adenosine A2A receptor agonist, CGS21680, upregulate CD39 and CD73 expression through E2F-1 and CREB in regulatory T cells isolated from septic mice, Int. J. Mol. Med. 38 (3) (2016) 969–975.

[80] J.L. Jeffrey, K.V. Lawson, JP. Powers, Targeting metabolism of extracellular nucleotides via inhibition of ectonucleotidases CD73 and CD39, J. Med. Chem. 63 (22) (2020) 13444–13465.
[81] I.E. Glykofridis, J.C. Knol, J.A. Balk, D. Westland, T.V. Pham, S.R. Piersma, et al., Loss of FLCN-FNIP1/2 induces a non-canonical interferon response in human renal tubular epithelial cells, eLife 10 (2021).
[82] L. El-Houjeiri, E. Possik, T. Vijayaraghavan, M. Paquette, J.A. Martina, J.M. Kazan, et al., The transcription factors TFEB and TFE3 link the FLCN-AMPK signaling axis to innate immune response and pathogen resistance, Cell Rep. 26 (13) (2019) 3613–3628, e6.
[83] T.K. Choueiri, W.G. Kaelin, Targeting the HIF2–VEGF axis in renal cell carcinoma, Nat. Med. 26 (10) (2020) 1519–1530.
[84] A.J. Armstrong, S. Halabi, T. Eisen, S. Broderick, W.M. Stadler, R.J. Jones, et al., Everolimus versus sunitinib for patients with metastatic non-clear cell renal cell carcinoma (ASPEN): a multicentre, open-label, randomised phase 2 trial, Lancet Oncol. 17 (3) (2016) 378–388.
[85] Y.M. Rustum, S. Chintala, F.A. Durrani, A. Bhattacharya, Non-coding micro RNAs and hypoxia-inducible factors are selenium targets for development of a mechanism-based combination strategy in clear-cell renal cell carcinoma-bench-to-bedside therapy, Int. J. Mol. Sci. 19 (11) (2018).
[86] C.S. Li, Z.Z. Lu, D.L. Fang, W.J. Zhou, J. Wei, Immune-related long non-coding RNAs can serve as prognostic biomarkers for clear cell renal cell carcinoma, Transl. Androl. Urol. 10 (6) (2021) 2478–2492.
[87] J. Chen, C. Yao, N. Qiao, Y. Ge, J. Li, Y. Lin, et al., Development and validation of a PBRM1-associated immune prognostic model for clear cell renal cell carcinoma, Cancer Med. 10 (19) (2021) 6590–6609.
[88] Z. Zhang, E. Lin, H. Zhuang, L. Xie, X. Feng, J. Liu, et al., Construction of a novel gene-based model for prognosis prediction of clear cell renal cell carcinoma, Cancer Cell Int. 20 (2020) 27.
[89] Y. Zhang, X. Zhang, X. Lv, M. Zhang, X. Gao, J. Liu, et al., Development and validation of a seven-gene signature for predicting the prognosis of lung adenocarcinoma, Biomed. Res. Int. 2020 (2020), 1836542.
[90] W. Shao, Z. Yang, Y. Fu, L. Zheng, F. Liu, L. Chai, et al., The pyroptosis-related signature predicts prognosis and indicates immune microenvironment infiltration in gastric cancer, Front. Cell Dev. Biol. 9 (2021), 676485.
[91] X. Yin, Z. Wang, J. Wang, Y. Xu, W. Kong, J. Zhang, Development of a novel gene signature to predict prognosis and response to PD-1 blockade in clear cell renal cell carcinoma, Oncoimmunology 10 (1) (2021), 1933332.
[92] Y. Hong, M. Lin, D. Ou, Z. Huang, P. Shen, A novel ferroptosis-related 12-gene signature predicts clinical prognosis and reveals immune relevancy in clear cell renal cell carcinoma, BMC Cancer 21 (1) (2021) 831.
[93] Q. Peng, Y. Zhou, L. Jin, C. Cao, C. Gao, J. Zhou, et al., Development and validation of an integrative methylation signature and nomogram for predicting survival in clear cell renal cell carcinoma, Transl. Androl. Urol. 9 (3) (2020) 1082–1098.